Research Square

Preprints are preliminary reports that have not undergone peer review.
They should not be considered conclusive, used to inform clinical practice,
or referenced by the media as validated information.

pH-clock programmed autonomous bidirectional actuation and optical modulation of a multi-stimuli-responsive hydrogel

Debapratim Das

ddas@iitg.ac.in

ddas@iitg.ac.in https://orcid.org/0000-0003-2295-0966

Sampurna Routray

Indian Institute of Technology Guwahati

Priyam Das

Indian Institute of Technology Guwahati

Malay Baroi

Indian Institute of Technology Guwahati https://orcid.org/0009-0003-5332-4009

Article

Keywords:

Posted Date: August 11th, 2026

DOI: https://doi.org/10.21203/rs.3.rs-10471605/v1

License: This work is licensed under a Creative Commons Attribution 4.0 International License.
Read Full License

Additional Declarations: There is **NO** Competing Interest.

pH-clock programmed autonomous bidirectional actuation and optical modulation of a multi-stimuli-responsive hydrogel

Sampurna Routray, Priyam Das, Malay Kumar Baroi, Debapratim Das*

Department of Chemistry, Indian Institute of Technology Guwahati, North Guwahati, Assam 781039, India. Email: ddas@iitg.ac.in

Abstract

Harnessing chemical reaction networks to regulate hydrogel actuators offers a promising route toward bioinspired smart materials with autonomous and programmable behaviours. Herein, we report a multi-stimuli-responsive bilayer hydrogel actuator that responds to both pH and metal ions. The bilayer actuator comprises two polyacrylamide-based layers, one functionalised with 1-vinylimidazole (VIm) and the other with methacrylic acid (MAA). The orthogonal ionizable groups impart distinct swelling responses across different pH regimes, enabling programmable bidirectional motion, while VIm's metal-ion coordination provides an additional stimulus-responsive mode. To emulate adaptive processes found in nature, the actuator was coupled with a newly developed autonomous NaOH–Sultone pH-clock. Addition of NaOH rapidly raises the pH to ~12, while the slower hydrolysis of Sultone generates sulfonic acid and gradually returns the system to the acidic region (~2.5), thereby creating a broad temporal pH window. Under these dynamically evolving chemical conditions, the bilayer displayed self-regulated bidirectional motion without any external intervention, converting transient chemical signals into programmed mechanical deformation. The pH-clock enables autonomous bidirectional actuation, driving the actuator from 0° to 140°, back through 0°, and subsequently to -135°. To further enhance its biomimetic character, a pH-responsive aggregation-induced emission luminogen (AIEgen) was incorporated into the VIm-containing layer. The resulting material exhibited autonomous, time-dependent fluorescence modulation synchronised with the evolving pH environment, thereby coupling macroscopic motion with transient luminescence. By integrating a new pH-clock with a multi-responsive hydrogel architecture, the system achieved simultaneous regulation of mechanical actuation and optical output, producing adaptive, life-like behaviour and providing a versatile platform for next-generation autonomous soft materials.

1. Introduction

Motion is a fundamental feature of living systems, from plant tropism to animal taxis, where organisms autonomously sense and respond to environmental stimuli.[1-4] A classic example is sunflower heliotropism, in which flower heads track the Sun during the day and reorient eastward at night, demonstrating coordinated adaptation across space and time.[5,6] Inspired by such dynamic and autonomous behaviours in nature, stimuli-responsive materials and actuating systems have attracted significant attention in recent years.[7-9] In this context, adaptable, flexible soft materials such as hydrogel actuators exhibit lifelike attributes.[10-13] Their biomimetic nature makes them preferred choices for constructing bioinspired, stimuli-responsive, self-regulated smart materials.[14-16] Self-regulated hydrogel actuators operate by converting continuous external environmental cues into time-dependent macroscopic mechanical deformation.[17] The fundamental mechanism of autonomous actuation arises from the temporally asymmetric swelling or deswelling of the hydrogel, which is driven by continuous changes in external stimuli such as moisture, temperature, pH, light, redox state, or coordination with metal ions.[18-23]

The continuous motion in actuator systems can be achieved by coupling chemical reaction networks (CRNs) with hydrogels. Their intrinsic dynamics generate complex non-equilibrium temporal behaviour, thereby imparting adaptive biomimetic features to the actuators. Periodic changes in microscopic chemical conditions (pH, redox potential, ionic strength, etc) can lead to autoregulatory macroscopic deformations in hydrogels.[10,24,25] Fusi et al. reported an excellent autonomous soft robot that operated based on the CRN. Integration of a self-decarboxylating, pH-flipping acid into a bilayer hydrogel enabled autonomous operation.[26] Paikar et al. presented a life-inspired smart polyacrylamide-based hydrogel actuator that self-regulated with the autocatalytic front of thiols. However, the system's actuation mechanism was intrinsically irreversible.[27] Further, the same group successfully demonstrated the spatiotemporal regulation of the reversible hydrogel actuators using a more advanced approach.[28] Although the reported CRN-driven systems exhibit promising and efficient actuation performance, their motion is generally limited to a single direction. Typically, the actuator bends from its initial position to a maximum deflection and subsequently returns to its original state under the control of the CRN. However, autonomous actuation that drives the actuator beyond its initial position to the opposite extreme (bidirectional actuation) has not yet been charted. They also demand sophisticated CRN-based strategies and the incorporation of complex chemical constituents. The development of autonomous, lifelike motion remains limited by system complexity; therefore, robust yet chemically simple platforms capable of reversible, bidirectional responses are urgently needed. To this end, simpler pH-clocks that generate temporal pH variations can serve as a more convenient alternative.[29-36] Again, most pH-cycles

operate over narrower pH ranges, limiting their use for macroscopic material motions. A pH-clock spanning a broad pH window (≈3–11) is crucial for efficiently transducing chemical signals from the homogeneous solution phase to the macroscopic bulk material. Thus, there remains significant scope for the design and fabrication of stimulus-responsive, self-regulated hydrogel actuators that can exhibit time-controlled, bidirectional, autonomous motion.

In what follows, we have designed a bioinspired bilayered multi-stimuli-responsive hydrogel actuator that exhibits pH-clock-guided, reversible, autonomous bidirectional motion. This objective was achieved by incorporating two distinct components, 1-vinylimidazole (VIm) and methacrylic acid (MAA), into two individual layers of a polyacrylamide hydrogel matrix (Figure 1). The pH-switchable ionisation properties of the components across reversible pH ranges introduced bidirectional responsiveness to the system. Furthermore, we developed a new NaOH-sultone (NaOH-Sul) dynamic pH-cycle and demonstrated a pH-clock-guided, autonomous, time-regulated bidirectional actuation driven by differential swelling. Moreover, to enhance the system's environmental fidelity and biomimetic relevance, we deliberately incorporated a pH-responsive aggregation-induced emission luminogen (AIEgen) tetraphenylethylene (TPE) derivative. The doped material mimicked the transient switch-on/off bioluminescent behaviour of marine life.[37]

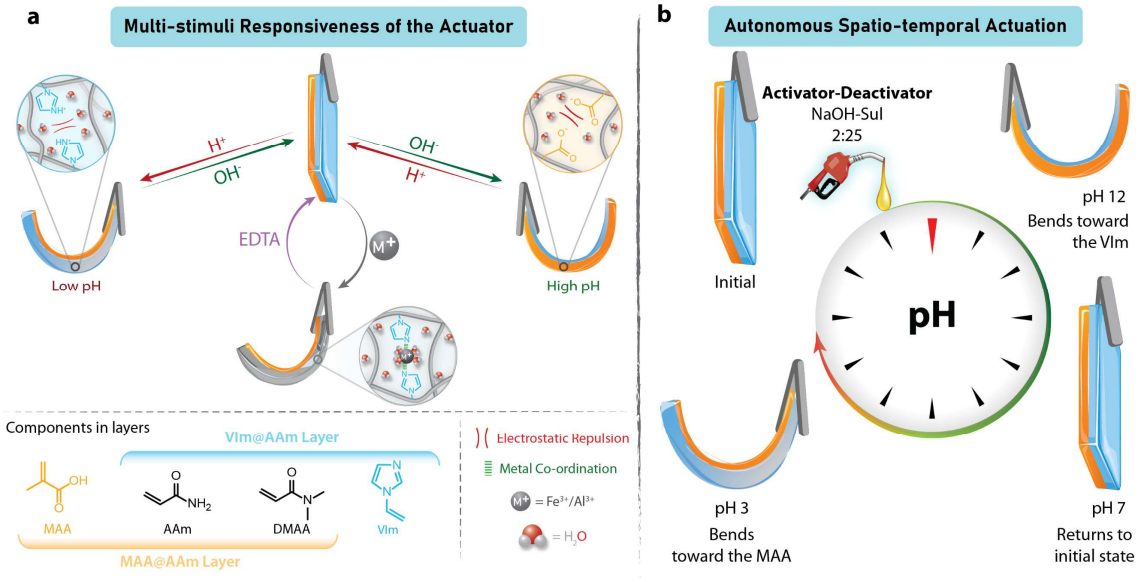


FIGURE 1| Schematic representation of the autonomous bidirectional biomimetic hydrogel actuator with multi-stimuli responsiveness. **a,** Graphical presentation of the structural components of the bilayer hydrogel and its multi-stimuli-responsiveness. **b,** Schematic presentation of the autonomous bidirectional actuation of the actuator driven by NaOH-Sultone pH-clock.

Results and discussion

Design, preparation, and characterisation of the actuator

To fabricate a lifelike autonomous actuator, our primary requirement was to design and develop a hydrogel architecture capable of demonstrating multi-stimuli responsiveness. So far, the stimuli used for multi-stimuli-responsive hydrogel actuators are interconnected, as in the case of light and heat.[38,39] In such cases, mechanical deformation exhibits limited independent control over individual stimuli. For example, Wang et al. reported a soft actuator that can exhibit reversible deformation in response to light, temperature, and humidity.[40] Xiao et al. fabricated a multi-stimuli-driven actuator that demonstrated responsiveness to two mutually related stimuli – temperature and humidity.[41] In both instances, the mechanisms of stimulus activation are interdependent. Changing one stimulus affects the other, thereby leveraging mutual dependence in such systems. With these considerations in mind, the bilayered hydrogel architecture in the present case was designed to respond to two mutually unrelated stimuli – pH and metal ions.

Accordingly, the system was first engineered to function across all pH conditions. A careful integration of components selectively sensitive to each stimulus should result in controlled, programmable actuation behaviour. To accomplish the goal, we selected two individual components, 1-vinylimidazole (VIm) and methacrylic acid (MAA) (Figure 1). Both components can respond selectively to two orthogonal stimuli, pH and metal ions. Firstly, they exhibit strong pH-dependent behaviour due to their ionisable functional groups. VIm contains a weakly basic imidazole group with a pKa of approximately 6.0–6.5.[42] It readily accepts protons in acidic environments (pH < 6) and loses them in basic conditions (pH > 7). Whereas MAA, having a pKa of 4.65,[43] loses its protons in the basic range. Thus, the distinct ionisation properties of the individual components can endow a hydrogel actuator with pH responsiveness.[44-47] In addition to their pH-responsive properties, these moieties exhibit versatile coordination chemistry. This enables them to bind effectively to metal ions. Herein, utilising the pH- and metal-ion responsiveness of the components, we established our hydrogel actuator by integrating them into separate layers of a bilayered polymeric matrix. The resulting bilayer exhibited controlled motion in response to two orthogonal stimuli: pH and metal ions. The polymeric matrix of both layers consisted of acrylamide (AAm) and N, N–dimethylacrylamide (DMAA) crosslinked by N, N'-methylenebisacrylamide (MBAA). VIm and MAA were incorporated into the respective layers of the bilayered system with the help of a free radical polymerisation technique (Supplementary Information).

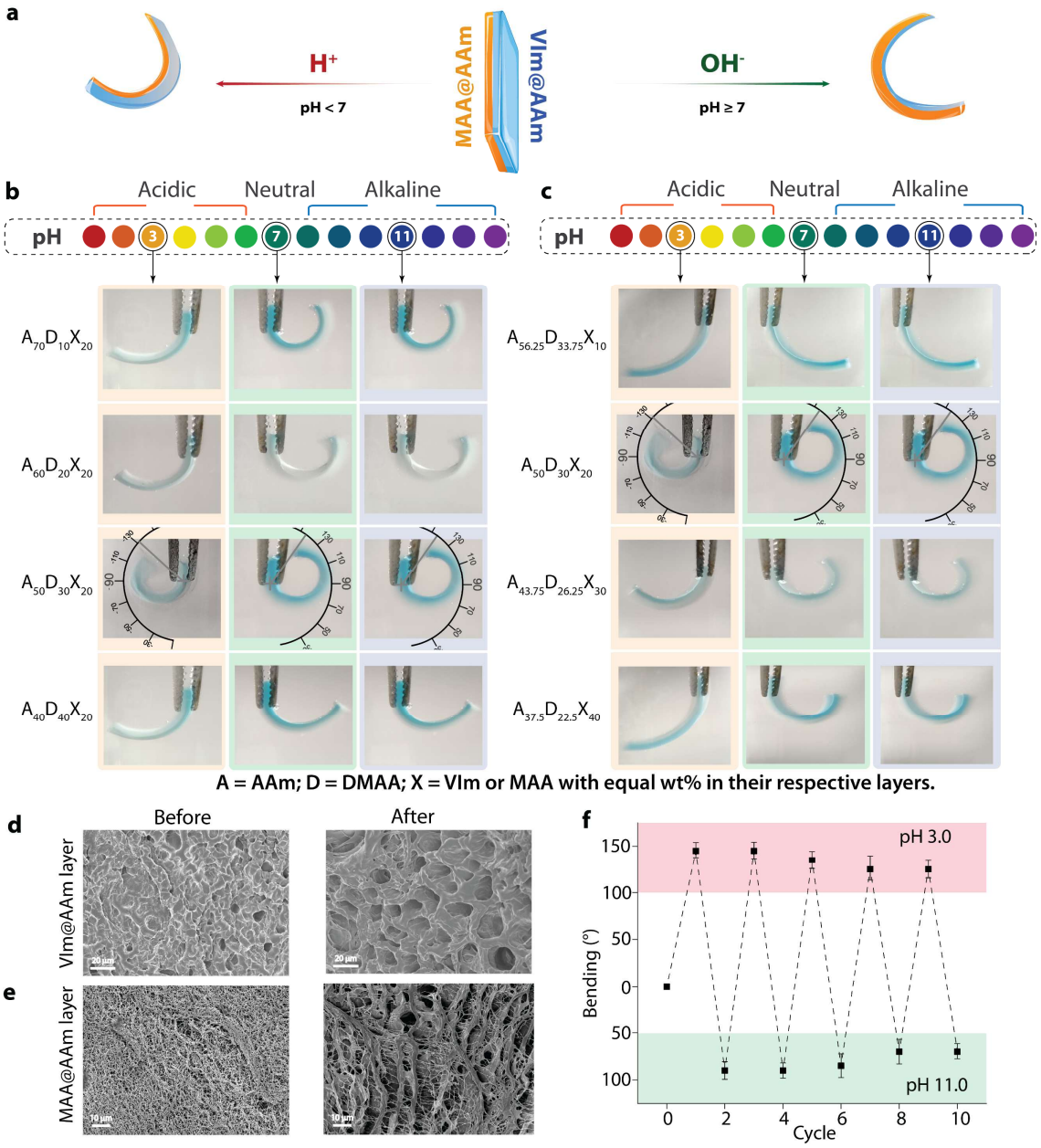


FIGURE 2| Optimisation of the composition of the hydrogel actuator. **a,** Graphical representation of the pH-dependent actuation of the HA. **b-c,** Photographs of the maximum bending achieved at three different pH (3, 7, and 11) by **b,** $A_mD_nX_{20}$, and **c,** $A_mD_nX_o$ bilayered hydrogels with m:n fixed at 5:3. The negative scale on the protractor is purposefully added to easily distinguish between the direction of the rotation. **d-e,** FESEM images of the individual active layers before and after achieving maximum bending. **d,** in pH 3 and **e,** in pH 11 solutions. The bilayer actuators were prepared using one layer of polyacrylamide and another with polyacrylamide and VIm or MAA. **f,** Repeatability of the actuation in pH 3 and pH 11 by the bilayer actuator ($A_{50}D_{30}X_{20}$). All experiments were performed at room temperature.

We prepared a library of actuators by varying the weight percentages of the hydrogel's constituents. The hydrogels are named as $A_mD_nX_o$, where A, D, and X represent AAm, DMAA, and the dopants (VIm or MAA), respectively, while m, n, and o denote the corresponding wt% of these components. Firstly, the dopant (X) weight percentage in the respective layers was kept constant at 20 wt%, while the

concentrations of AAm and DMAA were varied. A summary of the different combinations of $A_mD_nX_{20}$ hydrogels is provided in Table S1. The different hydrogels were then subjected to three discrete pH conditions (pH 3, 7, and 11), and the resulting swelling ratios at each pH were subsequently analysed (Figure S1A). It was observed that across all pH levels, the swelling ratio increased with higher AAm content, presumably due to the presence of hydrophilic amide groups that attract and retain water through hydrogen bonding.[48] An optimal degree of swelling is essential, as excessive swelling leads to mechanical instability, while inadequate swelling fails to generate the desired actuation or deformation. Thus, $A_{50}D_{30}X_{20}$ was considered the optimal composition, with 20 wt% dopant, to ensure effective and controlled actuation. Subsequently, to assess the effect of dopant concentration, we varied the dopant weight percentages while keeping the AAm-DMAA ratio fixed at 5:3 (Table S2). As shown in Figure S1B, $A_{50}D_{30}X_{20}$ exhibits the optimal swelling. Additionally, we also analysed the pH-dependent swelling behaviour of the individual layers of the optimised bilayered construct (Figure S2). The plot showed that the VIm@AAm layer exhibited a higher swelling ratio under acidic conditions, and the extent of swelling decreased as the pH increased. As expected, the imidazole groups in the VIm@AAm layer became protonated in the acidic medium, leading to greater swelling, and the lower extent of swelling in the neutral or alkaline range can be attributed to a lower degree of protonation. Similarly, the MAA@AAm layer exhibited a higher swelling ratio in the basic medium, and swelling decreased as pH diminished. The acid groups in the MAA@AAm layer deprotonated in alkaline conditions, resulting in greater swelling. These results confirmed that the selected dopants were suitable for pH-responsive bending performance in extreme conditions.

Next, we studied the extent of pH-dependent bending in actuators with different compositions (Figure 2a). As shown in Figure 2b and S3, $A_{50}D_{30}X_{20}$ exhibited the highest bending across all pH values. Under acidic, neutral, and basic conditions, the bending angles were observed to be -135°, 145°, and 145°, respectively. The hydrogels, $A_{70}D_{10}X_{20}$ and $A_{60}D_{20}X_{20,}$ with a higher concentration of hydrophilic AAm, led to the excessive swelling of the system, eventually leading to a lower bending deformation. On the other hand, the hydrogel $A_{40}D_{40}X_{20,}$ with a lower AAm content, exhibited lower mechanical stability, resulting in minimal bending. Subsequently, the bending of the other hydrogels with a fixed AAm–DMAA ratio (5:3) and varying dopant content was also studied under similar pHs (Figure 2c and S4). Notably, the $A_{50}D_{30}X_{20}$ hydrogel exhibited the highest bending angles among all the combinations. The dopant concentration in the bilayered polymeric matrix significantly affected the bending behaviour. With a lower dopant content (10–20 wt%), the desired actuation was not achieved. On the other hand, higher dopant concentrations (40 wt%) led to systems with lower polymeric matrix content; proper gel network formation was hindered, resulting in loss of structural integrity and lower bending. Based on these observations, it was clear that

$A_{50}D_{30}X_{20}$ provides the optimal composition, with prominent pH-responsive actuation. Hereafter, the hydrogel $A_{50}D_{30}X_{20}$ will be referred to as the hydrogel actuator (HA).

Next, to characterise the HA, FTIR spectra of each constituent layer and the integrated bilayered construct were recorded and depicted in Figure S5. A table summarising each layer's absorption peaks and the corresponding functional groups is provided in the Supplementary Information (Table S3). The presence of the characteristic absorption bands of the individual layers within the bilayered construct confirmed the successful fabrication of the HA comprising both layers.[49-51] Rheological studies revealed a higher storage modulus (G') for the HA compared with the individual layers (Figure S6-7). Integration of the individual layers into a bilayer architecture resulted in a substantial increase in the storage modulus. The synergistic interaction between the two layers resulted in a composite HA with sufficient strength and mechanical integrity to successfully support actuation behaviour.

Actuation in response to pH and metal ions

After optimizing the hydrogel actuator (HA), we investigated its response to pH and metal ions. Unlike conventional pH-responsive bilayer actuators, which operate only within a narrow pH range around the pKa of ionizable groups, our system was expected to exhibit bending across the entire pH spectrum. Traditional designs contain a pH-responsive active layer and an inert passive layer, where pH-dependent ionisation induces charge generation, electrostatic repulsion, differential swelling, and actuation.[21,52] Consequently, their performance is restricted to a limited pH window, reducing operational versatility. In contrast, to achieve actuation across the entire pH window, we adopted a dual-active design strategy in which a basic component, VIm, was incorporated into one layer and an acidic component, MAA, into the opposing layer. This configuration enabled complementary ionisation responses under both acidic and basic conditions. First, the pH-responsiveness of the HA was studied under acidic conditions. The bilayered hydrogel was initially dipped in an aqueous solution at neutral pH. It showed very slow actuation, reaching 145° in 40 min. (Figure 2). However, when dipped in an aqueous solution of pH 11, HA bent equally within 10 min. The actuation in neutral water is presumably due to the deprotonation of MAA, which occurs even more rapidly when dipped in the pH 11 solution; thus, the actuation rate is faster under basic conditions. On the other hand, protonation of the VIm layer and subsequent swelling upon immersion in a pH 3 solution resulted in rapid actuation to 135° within 20 min (Figure 2). Upon exposure to acidic conditions, the imidazole groups on the polymeric chain protonate. This generated electrostatic repulsion within the polymer network, causing volumetric expansion of the VIm@AAm layer and bending it towards the MAA side (Figure 2).

The FESEM images of the VIm@AAm layer before and after the pH-dependent bending showed an increase in the pore size of the hydrogel matrix after the actuation (Figure 2d). This confirmed that protonation of VIm at acidic pH led to electrostatic repulsion, followed by the uptake of water molecules. FESEM analysis of the MAA@AAm layer also revealed an increase in pore size after bending, thereby validating the differential swelling behaviour at basic pH (Figure 2e). The generation of asymmetric swelling stress across the bilayer over a wide pH range resulted in bidirectional actuation. Thus, pH-guided directional actuation was achieved by incorporating two distinct pH-responsive components in separate layers of the design strategy. Additionally, we checked the reversibility of our actuator with changes in the pH of the aqueous medium (Figure 2f). The addition of a base to the bulk aqueous solution induced actuation toward the VIm side, and subsequent addition of acid triggered actuation in the opposite direction. This alternating process was repeated, and consistent actuation was observed over at least ten successive cycles. The bending angles of the actuator at both extreme pH conditions remained nearly the same across consecutive cycles. Consequently, this approach can be considered as a plausible alternative to overcome the inherent pH-window limitation of conventional single-component systems and can enable robust bidirectional actuation.

Given the exceptional ligand properties of imidazole and carboxylic acid groups, we hypothesised that metal ions could serve as an effective external stimulus. Metal–ligand coordination provides a direct, specific interaction mechanism that is generally unaffected by pH variations. We therefore anticipated that the coordination of metal ions selectively to a particular ligand could induce a controllable actuation response. Further, the addition of a reagent with a higher affinity for the metal ions could disrupt the metal-ligand coordination bond in the actuator, enabling reversible actuation (Figure 3a). A careful selection of metal ions and a specific reagent as a forward and backward stimulus, respectively, should generate an effective actuation behaviour. Metal ions that can either bind to imidazole or carboxylic acid groups were essential for an efficient bending performance. Subsequently, an appropriate reagent that preferably binds to the metal ion and cleaves the metal-ligand coordination bond, restoring the HA to its initial state, was also crucial.

Keeping all these criteria in mind, we selected ferric chloride (anhydrous) ($FeCl_3$) and aluminium chloride (anhydrous) ($AlCl_3$) metal ion salts for the forward actuation process, and ethylenediaminetetraacetic acid disodium salt dihydrate (EDTA) for the reversible actuation (Figure 3A). The metal ions were selected because both imidazole and carboxylate ions are hard ligands that prefer hard metals such as Fe^{3+} and Al^{3+}. EDTA, a hexadentate hard ligand, has a higher affinity for these metal ions and was thus chosen for reverse actuation.[53] Upon immersion in water, followed

by the addition of a $FeCl_3$ solution (to reach a final concentration of 10 mM), HA bent toward the MAA layer (Figure 3b). At neutral pH, the MAA remains protonated, preventing it from coordinating with metal ions. On the other hand, VIm remains in the unprotonated state, which allows it to act primarily as a neutral nitrogen donor, forming coordination bonds with Fe^{3+}. Coordination between imidazole groups and Fe^{3+} ions generated stable metal–ligand complexes. Furthermore, this led to an increase in charge density and, consequently, electrostatic repulsion-induced swelling of the VIm@AAm layer. Subsequently, the strain mismatch between the two layers led to actuation towards the MAA side.

To reverse the actuation, an aqueous EDTA solution (25 mM final concentration) was introduced into the system. EDTA functions as a stronger chelating agent that preferentially binds to metal ions over imidazole. Upon addition, EDTA disrupted the coordination interactions between Fe^{3+} ions and imidazole moieties by sequestering them into stable EDTA–Fe^{3+} complexes. This competitive complexation effectively broke the Fe^{3+}–imidazole coordination bonds. As a result, the crosslinking density associated with metal–ligand interactions decreased, leading to relaxation of the polymer network and recovery of the gel to its original state. Following this, the mechanical deformation of the bilayered actuator was also studied in the presence of $AlCl_3$ (Figure 3c). As in the case of actuation in the presence of $FeCl_3$, the pH of the bulk aqueous solution was kept neutral. Upon the addition of Al^{3+} ions (10 mM final concentration), the bilayered hydrogel exhibited a bending motion towards the MAA side. Further, upon the addition of EDTA, reversible bending was also achieved. The results were consistent with those observed for Fe^{3+} metal ions.

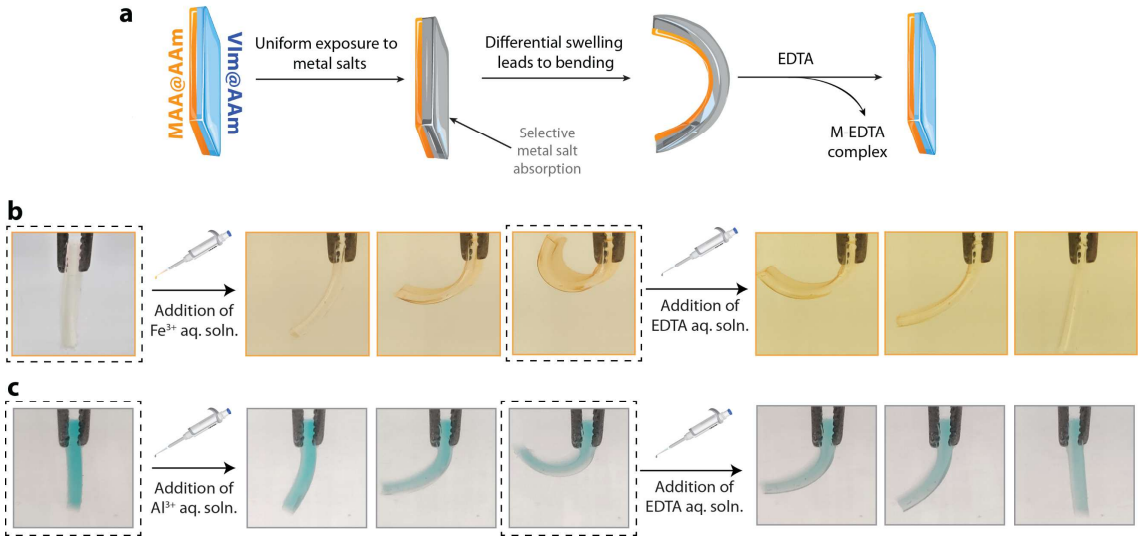


FIGURE 3| Reversible actuation of the hydrogel in response to metal ions and EDTA. **a,** Schematic illustration of the reversible actuation process in the presence of metal ions and EDTA. **b-c,** Images at different times from the reversible actuation achieved in the cases of **b,** Fe^{3+} and EDTA, **c,** Al^{3+} and EDTA. The experiments were performed at room temperature. The background colour in **b** is due to the presence of Fe^{3+} in the solution.

To validate the experimental observations in both cases above, several control experiments were performed. Two separate bilayered systems were prepared. Firstly, a bilayered hydrogel was prepared, with one side containing AAm and the other functionalised with VIm (VIm@AAm), which was immersed in the Fe^{3+} solution (Figure S8A). As in earlier observations, the VIm@AAm layer swelled, bending towards the AAm side. Further addition of EDTA to the system restored the hydrogel to its initial state. Another bilayer hydrogel containing an AAm and a MAA@AAm layer was subjected to a similar test. As shown in Figure S8B, no bending was observed in this case. As anticipated, methacrylic acid didn't form any coordination interaction with Fe^{3+}, and thus the system couldn't exhibit differential swelling behaviour. Even after adding EDTA, the system remained unchanged. A similar observation was also noted in the case of $AlCl_3$ metal salt (Figure S9).

In addition, we monitored changes in the pH of the bulk aqueous solution during the reversible bending motion of the HA. In the presence of Fe^{3+} ions, the bulk solution attained a pH of around 3. Upon adding the aqueous EDTA solution to the bulk, the pH value slightly rose to approximately 6.5 (Figure S10). From the results on pH-induced actuation discussed earlier, it was evident that pH-dependent actuation depends solely on pH values in the extreme regimes. While pH 3 lies in the extreme acidic region, pH 6.5 is not alkaline enough to contribute to actuation. Further, to demonstrate that the bending deformation was primarily due to Fe^{3+} rather than the acidic pH, we investigated the time course of bending deformation in each case (Figure S11). It was found that the bending in the case of Fe^{3+} ions was relatively faster (10 min) than in the presence of acid (20 min). These results confirmed that Fe^{3+}-mediated coordination was the dominant driving force for actuation, and the acidic pH generated by their hydrolysis was an additional contributing factor. Additionally, the metal-ion concentration-dependent actuation behaviour of the HA was investigated (Figure S12). It was observed that as the concentration of Fe^{3+} ions increased, the time required for mechanical bending decreased. This again confirmed that the actuation exhibited by the HA primarily depends on metal-ion binding in the system. Similarly, the pH of the system after the addition of $AlCl_3$ and EDTA changed minimally during reversible actuation (Figure S13). However, as discussed previously, pH-dependent actuation typically requires the pH to be at an extreme value. This indicated that actuation was achieved solely by the presence of Al^{3+} ions and EDTA.

Autonomous actuation

So far, we have demonstrated multi-stimulus-responsive behaviour in the bilayered hydrogel actuator. However, this forward-and-reverse actuation was achieved only by adding separate chemical triggers as forward and counter stimuli. Our larger goal is to achieve a life-like, autonomous, bidirectional actuation without the need for externally imposed consecutive stimuli.

This can be achieved if the to-and-fro motion is driven by a single chemical trigger that self-regulates time-coordinated opposing stimuli within the system. This strategy effectively emulates autonomous movements observed in living organisms, such as the sea anemone's tentacles, which contract when threatened and relax when safe.[54]

To autonomously regulate mechanical deformation across different pH regimes, a suitable pH-clock is required that exhibits time-controlled changes in pH. Since the bending motion was performed at extreme pH, we developed a NaOH-1,3-propanesultone (NaOH-Sul) pH-clock that operates over a wider pH range (Figure 4a). Herein, the solution is initially maintained at a low pH. The pH-clock is chemically triggered with the simultaneous addition of NaOH (activator) and Sul (deactivator). NaOH, being a strong alkali, rapidly increases the solution's pH to a high alkaline range. The system remains at alkaline pH as long as Sul permits. Over time, Sul undergoes slow ring-opening hydrolysis, gradually generating sulfonic acid and lowering the pH (Figure 4a).

The duration of this pH-clock can be suitably adjusted and reproduced, as it is adaptive to changes in the activator-to-deactivator ratio. Generally, a higher concentration of NaOH maintains the alkaline pH for a longer period before the deactivation kinetics begin to dominate. Conversely, at higher Sul concentrations, the solution remains alkaline for a shorter time before reaching acidic pH. This was confirmed by systematically running pH-clock experiments at different NaOH-Sul ratios. Initially, the Sul concentration was fixed at 25 mM, while the NaOH concentration was varied from 0.5 to 2.5 mM. Addition of NaOH registered a sharp jump in the pH (~ 12) followed by a gradual drop to a significantly acidic pH (~ 2.5) over a specific duration. The pH versus time plots for all cases were closely governed by different kinetics obtained from different concentration ratios. As can be seen from Figure 4b, with an increase in NaOH concentration, the lifetime of the pH-clock increases as the system stays at a higher pH for a longer period. Based on the results, we selected 2 mM NaOH as our working concentration and varied the Sul concentration from 20 to 40 mM. Understandably, a reverse effect was observed: an increase in Sul concentration as the cycle lifetime decreased from 70 min to 40 min (Figure 4c). Comparing pH-clock durations, we found that NaOH-Sul (2:25 mM) was optimal for our time-controlled, autonomous bidirectional actuation. The time-dependent pH variation was also monitored by measuring the temporal colour changes of the thymol blue (TB) dye under the influence of the pH-clock . TB exhibited orange colour before the onset of the pH-clock (pH ~ 2.8). When the pH-clock was triggered with NaOH-Sul (2:25 mM), TB instantly showed an intense blue colour (λ = 600 nm). Over time (80 min), the colour gradually transitioned from blue to green to yellow and finally to orange-yellow at the end of the cycle. Changes in the time-dependent absorbance values depict the corresponding variations in colour (Figure S14). Next, we checked the repeatability and adaptability of the established pH-clock . The pH-clock (2:25 mM NaOH-Sul) was

repeated over multiple cycles without significant damping (Figure 4d). It is worth noting that after initiating the pH-clock with 2:25 mM NaOH-Sul, only 2 mM NaOH was required to start the subsequent cycles. The remaining Sul in the system after the cycles was sufficient to run the subsequent cycles. After the 9th cycle, adding Sul was required to run the next cycle. This is an added advantage of the pH-clock where it is not needed to add the deactivator for every cycle. Also to be noted that the subsequent cycles should be started immediately after the completion of the previous cycle. Otherwise higher amount of NaOH will be required to raise the pH to the required level due to continuous drop in the pH of the system owing to sultone hydrolysis. To assess the adaptive nature of the pH-clock, several cycles were performed in the same solutions, with the NaOH-Sul ratio varied across cycles. The system showed high adaptability, as each cycle exhibited the expected lifetime without any noticeable dampening (Figure S15).

After establishing the NaOH–Sul pH clock, the bilayer hydrogel actuator (HA) was evaluated for autonomous actuation under dynamically evolving pH conditions (Figure 4e). Upon addition of the activator–deactivator pair (2:25 mM NaOH–Sul), the initial alkaline phase promoted deprotonation of the carboxylic acid groups, resulting in preferential swelling of the MAA@AAm layer and consequent bending of the bilayer toward the VIm side. This directional deformation persisted throughout the alkaline regime of the pH-clock (45–50 min), showing a maximum of 140° bending. The slightly lower maximum bending observed during the autonomous cycle (140° versus 145° under static conditions) arises from the finite swelling kinetics of the hydrogel relative to the continuously evolving pH profile. As the pH autonomously decreased and approached the pKa of VIm (~6.5, 60 min), protonation of the imidazole groups induced swelling of the VIm@AAm layer, generating an opposing stress that initiated reverse actuation. Reverse actuation became progressively more pronounced under increasingly acidic conditions (pH < pKa_{MAA} ~ 3.5, 65 min), where protonation of the methacrylic acid groups caused contraction of the MAA@AAm layer. The resulting inversion in differential swelling drove the bilayer through its neutral position (0°) into the opposite bending orientation, achieving a maximum bending of -135°.

Interestingly, comparison of the temporal evolution of pH and bending angle (Figure 4f) revealed a noticeable lag between the chemical stimulus and the mechanical response relative to the equilibrium bending observed under static pH conditions (Figure 2). This discrepancy is attributed to differences in the kinetics of pH variation and hydrogel swelling. Under static conditions, the actuator requires approximately 10 and 20 min to attain maximum bending in alkaline and acidic media, respectively. In contrast, during the pH-clock cycle, the pH changes continuously and rapidly, reaching values as low as pH 3 within 60 min. Consequently, the hydrogel network cannot equilibrate instantaneously with the evolving chemical environment, resulting in delayed

mechanical adaptation. By integrating the intrinsic pH responsiveness of the bilayer architecture with the NaOH–Sul pH clock, we achieved biomimetic autonomous bidirectional actuation (Supplementary Video S1). Although complete synchronisation between pH evolution and mechanical deformation was not attained, this limitation highlights an important avenue for future optimisation through improved material and actuator design.

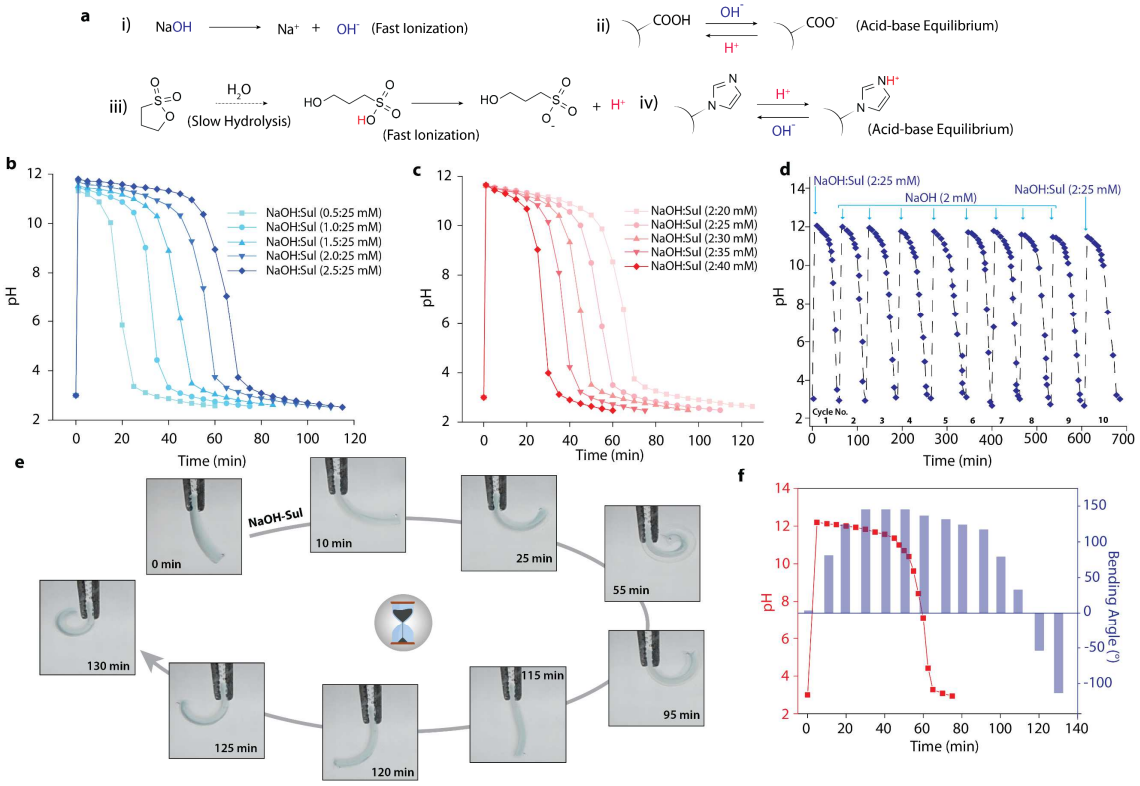


FIGURE 4| Establishing the NaOH-Sul pH-clock and autonomous actuation. **a,** Chemical reactions involved in the NaOH-Sul pH-clock and the consequent changes in different layers of HA. **b-c,** Optimising the NaOH-Sul pH clock. The change in pH with time with varying concentration of **b,** NaOH ([Sul] = 25 mM), and **c,** Sul ([NaOH] = 2 mM). **d,** Repeatability of the NaOH-Sul pH-clock over several cycles. **e,** Photographs of the actuator (HA) at different time points when it was subjected to 2:25 mM NaOH-Sul pH-clock showing the autonomous bidirectional bending with time (snapshots taken from video S1). **f,** Time-dependent changes in pH and bending angle during one cycle of autonomous motion of HA under the 2:25 mM NaOH–Sul pH-clock . All experiments were performed at room temperature.

pH-clock-instructed autonomous transient luminescent actuation

Bioluminescent organisms generate transient light emissions in response to environmental stimuli, often in conjunction with dynamic behavioural processes such as movement.[55] For example, deep-sea anglerfish coordinate body motion with temporal modulation of the luminescence emitted from their esca to attract prey. Regardless of their specific biological function, such adaptive responses are governed by underlying chemical reaction networks operating at the molecular level. Inspired by these natural systems, we sought to integrate transient emission behaviour with our bilayer actuator, which itself is driven by chemically programmed pH changes generated by the pH clock.

This prompted us to investigate whether autonomous actuation could be coupled with a transient luminescence program, thereby enabling the simultaneous regulation of motion and light emission through a common chemical reaction network.

To achieve this, we selected a pH-responsive derivative of tetraphenylethylene, tetrasodium salt of 4,4′,4″,4‴-(Ethene-1,1,2,2-tetrayl)tetrabenzoic acid (TPE4A), a well-established AIEgen.[56] TPE4A is a non-emissive water-soluble molecule that produces strong fluorescence under acidic pH (pH < 4.0). Firstly, to verify the pH-switchable property, we recorded the UV-Vis absorption, excitation and emission spectra under acidic and basic conditions for a fixed concentration of TPE4A (10 μM). TPE4A produced its characteristic absorption spectrum under acidic and basic media (λ_{max} = 350 nm) (Figure S16). The absorption spectra overlapped well with the excitation spectra for the respective pH (Figure S17). The emission spectra revealed no significant fluorescence under basic conditions, whereas a substantially intense broad band in the 400-650 nm range (λ_{em} = 500 nm) was generated under acidic conditions (Figure S18). The pH-dependent fluorescence was distinctly visualised under a 365 nm lamp. The acidic solution of TPE4A appeared strongly emissive with a cyan-green fluorescence, while the basic solution showed no emission (Figure S18 inset). The emission was highly pH-reversible and shuttled between on- and off-states over several cycles with alternating additions of acid and base (Figure 5a). The fluorescence decay profiles for emission at 500 nm were also recorded under respective conditions and have been summarised in Figure S19 and Table S4. The emission lifetimes were much higher in acidic media (3.710 ns) compared to that in basic condition (0.013 ns). All these experiments indicated that above the pKa, the tetraanionic molecule remained freely isolated in solution and remained non-emissive due to predominant non-radiative pathways. Below its pKa, the protonated TPE4A favoured an AIE effect arising from restricted intramolecular rotation.[57]

Next, we investigated the ability of TPE4A to exhibit transient fluorescence in the dynamically evolving pH environment generated by the pH-clock (Figure 5b). A complete pH-clock cycle was performed in a solution containing TPE4A, and the fluorescence intensity at 500 nm (I_{500}) was monitored over time. The emission profile closely tracked the system's instantaneous pH, demonstrating a strong correlation between the transient chemical environment and fluorescence output (Figure 5c). Upon addition of the trigger, the solution rapidly transitioned to an alkaline state, under which TPE4A exhibited minimal fluorescence, resulting in low I_{500} values. As the pH autonomously decreased over time, emissive species were progressively generated, leading to a gradual increase in fluorescence intensity. The emission reached its highest intensity toward the end of the cycle, where the system attained its most acidic pH values.

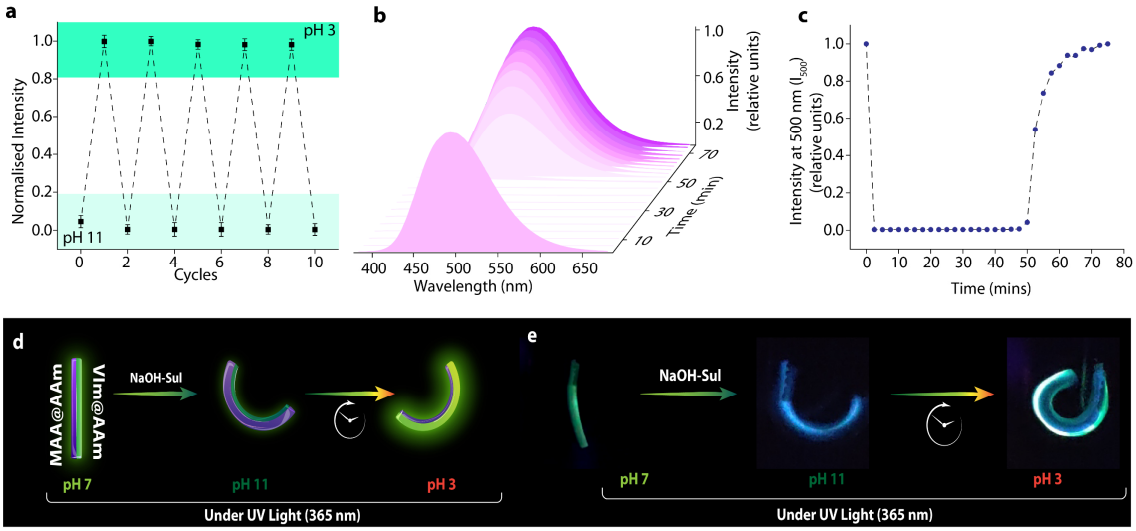


FIGURE 5| Colour-changing autonomous bidirectional actuation. **a,** pH-dependent reversible emission on-off switches exhibited by TPE4A for several cycles. [TPE4A] = 10 μM; λ_{ex} = 365 nm. **b-c,** Changes in **b,** emission profile and **c,** emission intensity of TPE4A with time under NaOH-Sul (2:25 mM) pH-clock. [TPE4A] = 10 μM; λ_{ex} = 365 nm. **d,** Schematic representation and **e,** Real-time images (snapshots from Video S2) showing autonomous NaOH–Sul (2:25 mM) pH-clock-instructed transient luminescent actuation of TPE4A@HA. All experiments were performed at room temperature.

We anticipated that the water-soluble TPE4A could be effectively immobilised within the VIm@AAm hydrogel matrix through a stable network of non-covalent intermolecular interactions. Accordingly, a fluorescent bilayer actuator, denoted TPE4A@HA, was fabricated by incorporating TPE4A into the VIm@AAm layer (see Supplementary Information). In its hydrated state, the bilayer exhibited negligible fluorescence. Upon exposure to an acidic stimulus, the actuator bent toward the MAA side, accompanied by the gradual emergence of fluorescence from the VIm layer. Conversely, treatment with a basic stimulus induced reverse bending toward the opposite direction and simultaneously quenched the fluorescence. Repeated alternate additions of acid and base produced synchronised bidirectional actuation and fluorescence on–off switching, demonstrating the coupled mechanical and optical responsiveness of the system (Figure S20). The emission spectra of TPE4A@HA revealed a broad and intense fluorescence band centred at 500 nm under acidic conditions, whereas negligible emission was observed in the basic state (Figure S21). To further characterise the photophysical behaviour, fluorescence lifetime measurements and quantum yield analyses were performed under both pH conditions, and the results are summarised in Figures S22–S23 and Tables S4–S5. These studies confirmed that TPE4A@HA remained essentially non-emissive in basic media. In contrast, under acidic conditions, protonation of TPE4A, together with its confinement within the hydrogel network, restricted intramolecular motion and promoted fluorescence via the restriction-of-intramolecular-rotation mechanism, resulting in a pronounced emission response.

When subjected to the pH clock, TPE4A@HA exhibited the previously described autonomous, time-programmed actuation together with a dynamically evolving fluorescence response (Figure 5d). At the onset of the clock cycle, the initially non-emissive actuator bent toward the VIm side, consistent with the differential swelling behaviour observed under alkaline conditions. As the pH autonomously decreased and the actuator began to reverse its orientation, a faint green fluorescence emerged from the VIm layer. The emission intensity progressively increased as the bilayer passed through its neutral position (0°) and continued bending toward the MAA side. By the end of the cycle, the VIm layer displayed a pronounced green luminescence concurrent with the maximum reverse deformation. Thus, the system demonstrated a unique form of chemically synchronised behaviour in which macroscopic shape transformation was coupled to transient fluorescence, producing a biomimetic display of adaptive motion and light emission under the control of an autonomous pH-clock (Supplementary Video S2).

To rationalise this behaviour, we propose a probable mechanism. At pH values above pKa_{VIm}, both the imidazole groups and TPE4A remain predominantly deprotonated, resulting in minimal intermolecular interactions and negligible fluorescence. As the pH decreases below pKa_{VIm}, protonation of the imidazole groups generates cationic sites within the hydrogel network that can electrostatically interact with the anionic TPE4A species. These interactions effectively immobilise TPE4A within the matrix, restricting intramolecular rotation and thereby activating fluorescence via the restriction-of-intramolecular-rotation (RIR) mechanism. As protonation progresses, the extent of electrostatic association increases, leading to a gradual increase in emission intensity. At later stages of the pH-clock cycle, where the pH becomes strongly acidic, TPE4A itself undergoes protonation. The resulting decrease in solubility may promote the formation of hydrophobic clusters or microdomains within the hydrogel network, further restricting molecular motion and enhancing fluorescence. The combined effects of electrostatic confinement and protonation-induced aggregation are therefore likely responsible for the progressively intensified emission observed as the pH-clock cycle approaches completion.

In summary, we have developed a bioinspired autonomous hydrogel actuator by integrating a chemical reaction network with a multi-stimuli-responsive bilayer hydrogel, enabling programmable bidirectional motion and dynamic luminescence under self-regulated chemical control. The actuator consists of two hydrogel layers containing 1-vinylimidazole (VIm) and methacrylic acid (MAA), respectively. The orthogonal ionizable groups impart distinct swelling behaviours across different pH regimes, resulting in programmable bidirectional actuation. Furthermore, the metal-ion coordination ability of VIm introduces an additional metal-responsive mode of operation. To emulate adaptive processes observed in nature, the actuator was coupled

with an autonomous NaOH–Sul pH clock. Under these dynamically evolving chemical conditions, the bilayer exhibited self-regulated bidirectional motion without continuous external intervention, effectively translating transient chemical signals into mechanical deformation. To further enhance its biomimetic character, the pH-responsive AIEgen TPE4A was incorporated into the VIm-containing layer. The resulting material displayed autonomous, time-dependent modulation of fluorescence that was synchronised with the evolving pH environment, thereby coupling macroscopic actuation with transient luminescence. The integration of a chemical reaction network with a multi-responsive hydrogel enabled the simultaneous regulation of motion and optical output, producing life-like adaptive behaviour. A notable advantage of this platform is its operational simplicity; whereas most CRN-based autonomous polymer systems rely on intricate multicomponent reaction mixtures, autonomous control in our system is achieved using a simple combination of NaOH and Sultone, substantially reducing operational complexity while retaining dynamic functionality. Overall, this work establishes a versatile framework for developing autonomous soft materials with potential applications in biomimetic robotics, adaptive materials, smart sensors, and responsive devices that operate in complex, dynamic environments.

Methods

Materials

Acrylamide (AAm) and Ammonium persulphate (APS) were procured from SRL, India. N, N-dimethylacrylamide (DMAA) (stabilised with MEHQ), 1-vinylimidazole (VIm) and methacrylic acid (MAA) (stabilised with MEHQ) were purchased from TCI, India. N, N′-methylenebisacrylamide (MBAA) and 1,3-propanesultone were also purchased from TCI. N, N, N′, N ′-tetramethylethylenediamine (TEMED) and aluminium chloride (anhydrous) were procured from Sigma-Aldrich, India. Ferric chloride (anhydrous) and E.D.T.A. disodium salt dihydrate were purchased from Rankem, India. 4, 4', 4'', 4'''-(ethene-1,1,2,2-tetrayl)tetrabenzoic acid (TPE4A) was purchased from BLD Pharmatech (India) Private Limited. All of the materials were used without further purification.

Characterisation

Morphologies of the hydrogels were characterised using field-emission scanning electron microscopy (FESEM) images obtained on a Gemini SEM 300 (Zeiss) instrument. The samples were freeze-dried before and after the pH-responsive bending deformation. The freeze-dried solid samples were then mounted on a silicon wafer through double-sided carbon tape for the FESEM analysis. FTIR spectra of the individual hydrogel layers and the bilayer actuator were recorded using a Nicolet iS50 FTIR spectrophotometer (PerkinElmer) under ambient conditions over the spectral range of 4000–400 cm^{-1}. Rheological studies of the various hydrogel samples were conducted using

an Anton Paar MCR 102 rheometer equipped with a 20 mm parallel-plate (0.5 mm zero-gap) measuring system at 25 °C.

Fabrication of multi-stimuli-responsive bilayered HA

The bilayered hydrogel was fabricated by the in situ radical polymerisation technique. Firstly, 50 mg of AAm (50 wt%), 30 mg of DMAA (30 wt%), 20 mg of VIm (20 wt%) and 4 mg of crosslinker MBAA were dissolved in 1 mL of deionised water (DI water). The solution was stirred for a few minutes. Further, 40 µL of a 4 wt% aqueous APS solution and 4 µL of TEMED were added to it to afford the prepolymeric solution for the first layer. The aqueous reaction mixture was then transferred to a glass mould and polymerised at 80 °C for 1 h. Next, the prepolymeric solution for the second layer was prepared similarly, except that VIm was replaced with MAA. The aqueous reaction mixture of the second layer was thereafter transferred onto the first layer and polymerised further for 2h. The other combinations of the bilayered hydrogels, $A_mD_nX_o$ (where A, D, and X represent AAm, DMAA, and the dopants (VIm or MAA), respectively, while m, n, and o denote the corresponding wt% of these components), were prepared in a similar manner. The compositions of the various hydrogel combinations are listed in Tables S1 and S2. The UV-Visible absorption and solution-based fluorescence spectra were recorded on Lambda 365+ (PerkinElmer) and Fluoromax 4+ (Horiba) spectrophotometers respectively.

pH-responsive actuation with HA

First, the base-responsive bending of the HA was analysed. The bilayered hydrogel was dipped in a beaker containing 90 mL of DI water. To it, 90 µL of 2 M NaOH solution was added. The actuation was then observed/recorded till the maximum bending is achieved. Similarly, for acid-responsive bending, the HA was dipped in a separate beaker (containing 90 mL DI water). 600 µL of 6 M HCl solution was added to it. The bending was then monitored till the maximum bending was achieved. Subsequently, in the pH-responsive reversibility experiment, equal amounts of NaOH and HCl were alternately added to the same beaker in consecutive cycles. The mechanical deformation was monitored after each addition.

Metal ion-responsive actuation with HA

A 0.9 M solution of $FeCl_3$ or $AlCl_3$ was prepared in DI water. The bilayered hydrogel was dipped in a beaker containing 89 mL of DI water, and then 1 mL of the salt solution was added and mixed with it to reach a final concentration of 10 mM. Upon reaching maximum binding with the metal ion, an aqueous EDTA solution was added to the bulk to achieve a final concentration of 25 mM. The actuator's reversibility in the presence of EDTA was then monitored till it returned to the original position.

pH-clock optimisation

In a 100 mL glass beaker, 90 mL of DI water was taken and acidified to pH 3.0 with 75 µL of 5 mM HCl. To it, the required volume/amount of NaOH (2 M stock solution) and solid 1,3-propanesultone were added. The solution was homogenised by stirring for 1 min, and the change of pH over time was noted. For subsequent repetitions, only the measured volume of NaOH was added to reinitiate the clock. For major experiments, the NaOH-Sul (2:25 mM) pH-clock was operated similarly in the presence of a fixed concentration of dye (thymol blue and TPE4A) or the actuator HA.

Autonomous pH-clock instructed actuation of the HA

The bilayered hydrogel was dipped in a beaker containing 90 mL of deionised water. To it, the required amount of NaOH and sultone stock solutions were added to maintain a concentration ratio of 2 M : 25 M. The autonomous change in the actuator's motion, along with the corresponding dynamic change in pH, was thereafter monitored over a given timeframe.

Fabrication of the fluorescent bilayered hydrogel actuator (TPE4A@HA)

The fabrication procedure followed similar steps to those of the optimised HA. During preparation, 50 µL of a 10 mM TPE4A solution was added to the prepolymeric mixture of the first layer (VIm@AAm). The solution was then transferred to a glass mould and allowed to polymerise at 80 °C for 1 h. Subsequently, the second layer (MAA@AAm) was prepared following similar steps. It was thereafter transferred onto the first layer and polymerised further for 2 h.

Autonomous pH-clock instructed transient fluorescent actuation of the HA

A similar experimental procedure to that of the autonomous regulation of the HA was employed. However, this time, the bilayered hydrogel with TPE4A trapped in the VIm@AAm layer was utilised for actuation. Bending deformation was observed under a 365 nm lamp over a defined period.

Solid-State Fluorescence measurements

The experiment was performed on a FLS1000 photoluminiscence spectrometer (Edinburgh) utilising a solid-state sample holder with a slit width of (E_x/E_m) = 2 nm/2 nm under λ_{ex} = 365 nm at 298 K. The TPE4A@HA was dipped in two different solutions of pH 3 and 11, respectively, for 1 h. Small pieces of the hydrogels, 10 mm × 2 mm, were then cut, taken out and placed in the solid sample holder, respectively, and the emission spectra were recorded.

Time-resolved photoluminescence and quantum yield measurements

The measurement was carried out on an Ultrafast-01-DD TCSPC lifetime system (Horiba) in a 3 mL quartz cuvette with a path length of 1 cm. For the pH-dependent measurements, the concentrations of TPE4A, HCl, and NaOH were maintained at 10 mM, 35 mM, and 2 mM, respectively. For time-resolved photoluminescence lifetime measurements, a 340 nm (~100 ps, 1 MHz repetition rate) diode laser was used for excitation. A deconvolution procedure was used to analyse the observed decays, which could be satisfactorily fitted by bi-exponential decay functions. A deconvolution procedure was used to analyse decays with a proper instrument response function obtained from a light scatterer (a suspension of TiO_2 particles in water). The fluorescence decays [I(t)] were analysed in general as a sum of exponentials,

$$I(t) = \sum B_i exp(-\frac{t}{\tau_i})$$

where, B_i and τ_i are the pre-exponential factor and fluorescence lifetime for the ith component, respectively. Reduced chi-square (χ^2) values and random distribution of the weighted residuals among data channels were used to judge the acceptance of the fits.

For solid-state time-resolved photoluminescence and quantum yield measurements, the TPE4A@HA samples were prepared in a similar manner to those of the solid-state fluorescence measurements. All the other parameters were kept fixed.

Acknowledgments

PD and MKB acknowledge the Ministry of Education (MoE), Government of India, for providing the Prime Minister's Research Fellowship. DD acknowledges funding from BRNS (58/14/05/2022), India.

Conflicts of Interest

The authors declare no conflicts of interest.

Data Availability Statement

The data supporting the findings of this study are available within the Article and its Supplementary Information. All raw data relevant to this manuscript are available upon request.

References

1 Pypka, M. & Siemianowski, O. Plant Tropism: Cue Detection and Control Over Growth Direction – The Many Ways for Plants to Explore and Exploit the Environment. *Bot. Rev.* **91**, 389-417 (2025).
2 Gilroy, S. Plant tropisms. *Curr. Biol.* **18**, R275-R277 (2008).
3 Rajewicz, W., Romano, D., Schmickl, T. & Thenius, R. Daphnia's phototaxis as an indicator in ecotoxicological studies: A review. *Aquat. Toxicol.* **265**, 106762 (2023).
4 Groneberg, A. H., Herget, U., Ryu, S. & De Marco, R. J. Positive taxis and sustained responsiveness to water motions in larval zebrafish. *Front. Neural Circuits* **9**, 9 (2015).
5 Brooks, C. J., Atamian, H. S. & Harmer, S. L. Multiple light signaling pathways control solar tracking in sunflowers. *PLoS biology* **21**, e3002344 (2023).

6 Vandenbrink, J. P., Brown, R. I., Harmer, S. L. & Blackman, B. K. Turning heads: The biology of solar tracking in sunflower. *Plant Sci.* **224**, 20-26 (2014).

7 Isapour, G. & Lattuada, M. Bioinspired Stimuli-Responsive Color-Changing Systems. *Adv. Mater.* **30**, 1707069 (2018).

8 Erb, R. M., Sander, J. S., Grisch, R. & Studart, A. R. Self-shaping composites with programmable bioinspired microstructures. *Nat. Commun.* **4**, 1712 (2013).

9 Wang, M., Lin, B.-P. & Yang, H. A plant tendril mimic soft actuator with phototunable bending and chiral twisting motion modes. *Nat. Commun.* **7**, 13981 (2016).

10 Chung, T. *et al.* Self-Regulating Hydrogel Actuators. *Chem. Rev.* **125**, 9053-9088 (2025).

11 Yang, J., Dong, Z., Liu, H. & Tian, Y. Bioinspired self-sensing hydrogel actuators: From mechanisms to applications. *Chem. Eng. J.* **512**, 162743 (2025).

12 Chen, C. *et al.* Bio-inspired multimodal soft actuator with environmental self-adaptation. *Nat. Commun.* **16**, 7630 (2025).

13 Guo, H. *et al.* Light-mediated communication in responsive materials ranging from individual self-oscillators to feedback-driven network. *Nat. Commun.* **16**, 11315 (2025).

14 Lee, J. E., Sun, Y.-C. & Naguib, H. E. Multifunctional soft actuator hybrids: a review. *RSC Appl. Polym.* **3**, 767-792 (2025).

15 Banerjee, H., Suhail, M. & Ren, H. Hydrogel Actuators and Sensors for Biomedical Soft Robots: Brief Overview with Impending Challenges. *Biomimetics* **3** (2018).

16 Dong, Y. *et al.* Multi-stimuli-responsive programmable biomimetic actuator. *Nat. Commun.* **10**, 4087 (2019).

17 Han, Z. & Zhang, J. Rapid-Responsive Hydrogel Actuators with Hierarchical Structures: Strategies and Applications. *ACS Appl. Polym. Mater.* **5**, 4605-4620 (2023).

18 Zhao, J. *et al.* From Sea Cucumbers to Soft Robots: A Photothermal-Responsive Hydrogel Actuator with Shape Memory. *ACS Appl. Mater. Interfaces* **17**, 6979-6986 (2025).

19 Jiang, X. *et al.* Super Stable Moisture-Responsive Actuator via Covalent Crosslinking for Efficient Personal Thermal Management. *Adv. Mater.* **37**, e07267 (2025).

20 Cho, Y. E., Park, J.-M., Song, W. J., Lee, M.-G. & Sun, J.-Y. Solvent Engineering of Thermo-Responsive Hydrogels Facilitates Strong and Large Contractile Actuations. *Adv. Mater.* **36**, 2406103 (2024).

21 van den Akker, W. P., van Benthem, R. A. T. M., Voets, I. K. & van Hest, J. C. M. Dampened Transient Actuation of Hydrogels Autonomously Controlled by pH-Responsive Bicontinuous Nanospheres. *ACS Appl. Mater. Interfaces* **16**, 19642-19650 (2024).

22 Nakahata, M., Takashima, Y., Hashidzume, A. & Harada, A. Redox-Generated Mechanical Motion of a Supramolecular Polymeric Actuator Based on Host–Guest Interactions. *Angew. Chem. Int. Ed.* **52**, 5731-5735 (2013).

23 Su, Y., Sugawara, A. & Uyama, H. Dual-Responsive Hydrogel Actuators with Anisotropic Metal Ion Cross-Linking and Polydopamine-Coated Cellulose Nanocrystals as Photothermal Fillers. *ACS Appl. Polym. Mater.* **7**, 15949-15959 (2025).

24 Greene, A. F. *et al.* Redox-Responsive Artificial Molecular Muscles: Reversible Radical-Based Self-Assembly for Actuating Hydrogels. *Chem. Mater.* **29**, 9498-9508 (2017).

25 Nan, M., Guo, K., Jia, T., Wang, G. & Liu, S. Novel Acid-Driven Bioinspired Self-Resettable Bilayer Hydrogel Actuator Mimicking Natural Muscles. *ACS Appl. Mater. Interfaces* **16**, 9224-9230 (2024).

26 Fusi, G., Del Giudice, D., Skarsetz, O., Di Stefano, S. & Walther, A. Autonomous Soft Robots Empowered by Chemical Reaction Networks. *Adv. Mater.* **35**, 2209870 (2023).

27 Paikar, A. *et al.* Spatiotemporal Regulation of Hydrogel Actuators by Autocatalytic Reaction Networks. *Adv. Mater.* **34**, 2106816 (2022).

28 Liao, F., George, A., Sui, X.-M. & Semenov, S. N. Autonomous Spatiotemporal Regulation of Reversible Hydrogel Actuators by Chemical Reaction Networks. *Adv. Mater.* **38**, e16185 (2026).

29 Das, P. *et al.* Time-Encoded Information Encryption with pH Clock Guided Broad-Spectrum Emission by Dynamic Assemblies. *Angew. Chem. Int. Ed.* **64**, e202414239 (2025).

30 Das, P., Baroi, M. K., Routray, S. & Das, D. Advanced Information Encryption via Parallel Time-Scale Modulation Using Broad-Spectrum Transient Colors From Organic Dyes. *ChemSystemsChem* **8**, e00067 (2026).

31 Das, T. *et al.* Temporally Programmed Hydrogelation of a Short Peptide Charge Transfer Complex. *Langmuir* **42**, 6512-6520 (2026).

32 Das, S., Das, T., Debnath, S., Scherman, O. A. & Das, D. pH Clock Guided Dynamic Broad Spectrum Multi-Color Fluorescence Modulation in Size-Oscillatory Vesicles. *Adv. Opt. Mater.* **12**, 2301422 (2024).

33 Chowdhuri, S. *et al.* Cumulative Effect of pH and Redox Triggers on Highly Adaptive Transient Coacervates. *Chem. Eur. J.* **29**, e202203820 (2023).

34 Das, S., Das, T., Das, P. & Das, D. Controlling the lifetime of cucurbit[8]uril based self-abolishing nanozymes. *Chem. Sci.* **13**, 4050-4057 (2022).

35 Das, S., Das, P., Dowari, P., Das, B. K. & Das, D. Bi-directional feedback controlled transience in Cucurbituril based tandem nanozyme. *J. Colloid Interface Sci.* **614**, 172-180 (2022).

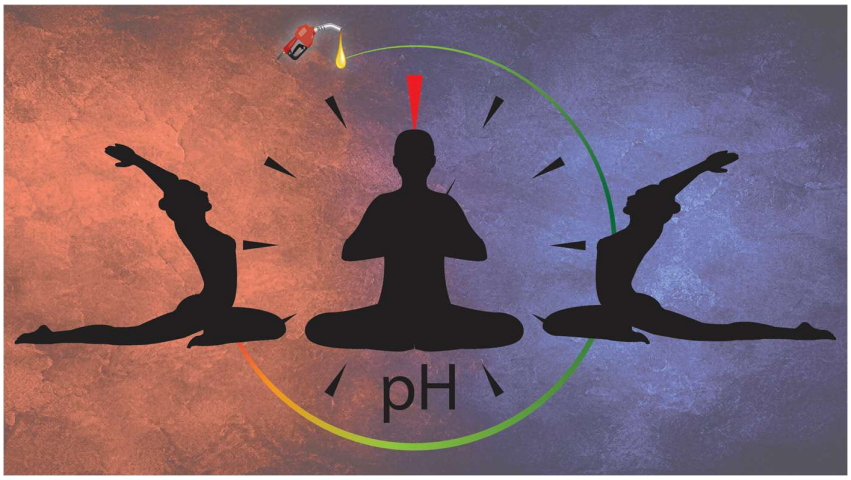
36 Das, P., Routray, S., Kushwaha, R., Baroi, M. K. & Das, D. Bioinspired chemoenzymatically controlled artificial light-harvesting nanoaggregates with multicolour transient emissions for time-gated information encryption. *Mater. Horiz.* **13**, 5022–5034 (2026).

37 Martini, S. & Haddock, S. H. D. Quantification of bioluminescence from the surface to the deep sea demonstrates its predominance as an ecological trait. *Sci. Rep.* **7**, 45750 (2017).

38 Wang, Y. *et al.* Ultrafast and Multi-Stimuli-Responsive MXene Soft Actuators via Heterostructure Design for Biomimetic Applications. *Adv. Funct. Mater.* **36**, e14386 (2026).

39 Hu, H., Nie, M., Galluzzi, M., Yu, X. & Du, X. Mimosa-Inspired High-Sensitive and Multi-Responsive Starch Actuators. *Adv. Funct. Mater.* **33**, 2304634 (2023).
40 Wang, W. *et al.* Multistimulus Responsive Actuator with GO and Carbon Nanotube/PDMS Bilayer Structure for Flexible and Smart Devices. *ACS Appl. Mater. Interfaces* **10**, 27215-27223 (2018).
41 Xiao, J. *et al.* Reprogrammable Multi-Responsiveness of Regenerated Silk for Versatile Soft Actuators. *Adv. Funct. Mater.* **34**, 2316301 (2024).
42 Asayama, S., Sekine, T., Kawakami, H. & Nagaoka, S. Synthesis of aminated poly(1-vinylimidazole) for a new pH-sensitive DNA carrier. *Nucleic Acids Symp. Ser. (Oxf)* **51**, 333-334 (2007).
43 Dong, H., Du, H. & Qian, X. Theoretical Prediction of pKa Values for Methacrylic Acid Oligomers Using Combined Quantum Mechanical and Continuum Solvation Methods. *J. Phys. Chem. A* **112**, 12687-12694 (2008).
44 Molina, M. J., Gómez-Antón, M. R. & Piérola, I. F. pH-dependence of the swelling capacity of poly(N-vinylimidazole) hydrogels. *Macromol. Chem. Phys.* **203**, 2075-2082 (2002).
45 Molina, M. J., Gómez-Antón, M. R. & Piérola, I. F. Factors driving the protonation of poly(N-vinylimidazole) hydrogels. *J. Polym. Sci. B Polym. Phys.* **42**, 2294-2307 (2004).
46 Díez-Peña, E., Quijada-Garrido, I. & Barrales-Rienda, J. M. On the water swelling behaviour of poly(N-isopropylacrylamide) [P(N-iPAAm)], poly(methacrylic acid) [P(MAA)], their random copolymers and sequential interpenetrating polymer networks (IPNs). *Polym.* **43**, 4341-4348 (2002).
47 Lally, S., Bird, R., Freemont, T. J. & Saunders, B. R. Microgels containing methacrylic acid: effects of composition on pH-triggered swelling and gelation behaviours. *Colloid Polym. Sci.* **287**, 335-343 (2009).
48 Bhadani, R. & Kumar, M. Studies on Water Absorbency of Polyacrylamide Hydrogels. *J. Mater. Sci. Eng. B.* **5** (2015).
49 Şarkaya, K. *et al.* Selective Extraction and Quantification of Hemoglobin Based on a Novel Molecularly Imprinted Nanopolymeric Structure of Poly(acrylamide-vinyl imidazole). *ACS Omega* **9**, 18458-18468 (2024).
50 Sekhavat Pour, Z. & Ghaemy, M. Preparation of poly(vinylalcohol)/poly(acrylamide-co-vinyl imidazole)/γ-Fe2O3 semi-IPN nanocomposite and their application for removal of heavy metal ions from water. *Polym. Adv. Technol.* **27**, 1557-1568 (2016).
51 Gupta, N. V. & Shivakumar, H. G. Investigation of Swelling Behavior and Mechanical Properties of a pH-Sensitive Superporous Hydrogel Composite. *Iran. J. Pharm. Res.* **11**, 481-493 (2012).
52 Li, B. *et al.* pH-responsive anisotropic hydrogels: A mini review from fabrication to simulation. *Sens. Actuators A Phys.* **392**, 116697 (2025).
53 Flora, S. J. S. & Pachauri, V. Chelation in Metal Intoxication. *Int. J. Environ. Res. Public Health* **7**, 2745-2788 (2010).
54 Menezes, C. & Thakur, N. L. Sea anemone venom: Ecological interactions and bioactive potential. *Toxicon* **208**, 31-46 (2022).
55 Schramm, S. & Weiß, D. Bioluminescence – The Vibrant Glow of Nature and its Chemical Mechanisms. *ChemBioChem* **25**, e202400106 (2024).
56 Bai, X. *et al.* Development of universal ultra-bright aggregation-induced emission fluorescent probes and applications in various forms. *Chem. Eng. J.* **522**, 168072 (2025).
57 Chen, J. & Tang, B. Z. in *Aggregation-Induced Emission: Fundamentals and Applications, Volumes 1 and 2* Vol. 1 (eds A. Qin & B.Z. Tang) 307-322 (2013).

Table of content graphic



Supplementary Files

This is a list of supplementary files associated with this preprint. Click to download.

- SupplementaryVideoS1.mp4
- SupplementaryVideoS2.mp4
- SupportingInformation.pdf